Inorg. Chem. **2004**, *43*, 2852−2858

Crystal Structures of Artificial Metalloproteins: Tight Binding of Fe^{III}(Schiff-Base) by Mutation of Ala71 to Gly in Apo-Myoglobin

Takafumi Ueno,[†] Masataka Ohashi,[‡] Masaharu Kono,[§] Kazuyoshi Kondo,[§] Atsuo Suzuki,[§] Takashi Yamane,[§] and Yoshihito Watanabe*,[||]

Research Center for Materials Science, Nagoya University, Nagoya 464-8602, Japan, Department of Structural Molecular Science, The Graduate University for Advanced Studies, Okazaki 444-8585, Japan, Department of Biotechnology and Biomaterial, Graduate School of Engineering, Nagoya University, and Department of Chemistry, Graduate School of Science, Nagoya University, Nagoya 464-8602, Japan

Received February 5, 2004

Apo-myoglobin (apo-Mb) and apo-A71GMb were successfully reconstituted with Fe^{III}(salophen) (**1**) (salophen = *N*,*N*′-bis(salicylidene)-1,2-phenilenediamine), Fe^{III}(3,3′-Me_2-salophen) (**2**), and Fe^{III}(5,5′-*t*-Bu_2-salophen) (**3**). The crystal structure of **2·apo-A71GMb** shows the tight binding of the complex in the Mb cavity, while in wild-type apo-Mb it is highly disordered due to the steric repulsion with Ala71. Furthermore, the structure of **2·apo-A71GMb** suggests a possible accommodation of a small substrate in the cavity. In fact, the cyanide association rate constant of **2·apo-A71GMb** is 216-fold larger compared to that of **2·apo-Mb**. These results provide us principles for the noncovalent fixation of synthetic metal cofactors at the desired positions in protein matrixes.

Introduction

Composites of metal ions and proteins are attractive biomolecules for a wide range of applications, e.g., materials,[1−3] sensors,[4,5] and catalysts.[6−8] Incorporation of synthetic metal cofactors into proteins is one of the powerful tools to prepare the composites.[9] Typical examples of the traditional techniques for the incorporation of the cofactors into protein matrixes are chemical modifications of either amino acid residues[10,11] or native cofactors[12−15] and random insertion of metal complexes.[16] However, these methods have limitations with respect to the modification of the position and number of amino acid residues or metal cofactors as well as difficulties in synthesizing functional groups to be attached. Thus, it is very hard to place the synthetic cofactor at the desired position in any protein matrix.

It would be nice if we could introduce synthetic metal cofactors as simple as the heme prosthetic group that is tightly bound in the cavity of heme enzymes and proteins.[17] For example, the affinity of heme for apo-myoglobin (apo-Mb) results from (i) hydrogen bond and hydrophobic interactions between the protein and heme and (ii) the coordina-

* To whom correspondence should be addressed. E-mail: yoshi@nucc.cc.nagoya-u.ac.jp. Phone: +81-52-789-3049. Fax: +81+52+789+2953.
[†] Research Center for Materials Science, Nagoya University.
[‡] The Graduate University for Advanced Studies.
[§] Department of Biotechnology and Biomaterial, Graduate School of Engineering, Nagoya University.
[||] Department of Chemistry, Graduate School of Science, Nagoya University.

(1) Meldrum, F. C.; Wade, V. J.; Nimmo, D. L.; Heywood, B. R.; Mann, S. *Nature* **1991**, *349*, 684−687.
(2) Douglas, T.; Young, M. *Nature* **1998**, *393*, 152−155.
(3) Ishii, D.; Kinbara, K.; Ishida, Y.; Ishii, N.; Okochi, M.; Yohda, M.; Aida, T. *Nature* **2003**, *423*, 628−632.
(4) Dragnea, B.; Chen, C.; Kwak, E.-S.; Stein, B.; Kao, C. C. *J. Am. Chem. Soc.* **2003**, *125*, 6374−6375.
(5) Braha, O.; Walker, B.; Cheley, S.; Kasianowicz, J. J.; Song, L.; Gouaux, J. E.; Bayley, H. *Chem. Biol.* **1997**, *4*, 497−505.
(6) Xiao, Y.; Patolsky, F.; Katz, E.; Hainfeld, J. F.; Willner, I. *Science* **2003**, *299*, 1877−1881.
(7) Benson, D. E.; Wisz, M. S.; Hellinga, H. W. *Curr. Opin. Biochem.* **1998**, *9*, 370−376.
(8) Lu, Y.; Berry, S. M.; Pfister, T. D. *Chem. Rev.* **2001**, *101*, 3047−3080.
(9) Qi, D.; Tann, C.-M.; Haring, D.; Distefano, M. D. *Chem. Rev.* **2001**, *101*, 3081−3111.
(10) Davies, R. R.; Distefano, M. D. *J. Am. Chem. Soc.* **1997**, *119*, 11643−11652.
(11) Sigman, D. S.; Bruice, T. W.; Mazumder, A.; Sutton, C. L. *Acc. Chem. Res.* **1993**, *26*, 98−104.
(12) Wilson, M. E.; Whitesides, G. M. *J. Am. Chem. Soc.* **1978**, *100*, 306−307.
(13) Hayashi, T.; Hitomi, Y.; Ando, T.; Mizutani, T.; Hisaeda, Y.; Kitagawa, S.; Ogoshi, H. *J. Am. Chem. Soc.* **1999**, *121*, 7747−7750.
(14) Hu, Y.-Z.; Tsukiji, S.; Shinkai, S.; Oishi, S.; Hamachi, I. *J. Am. Chem. Soc.* **2000**, *122*, 241−253.
(15) Collot, J.; Gradinaru, J.; Humbert, N.; Skander, M.; Zocchi, A.; Ward, T. R. *J. Am. Chem. Soc.* **2003**, *125*, 9030−9031.
(16) Marchetti, M.; Mangano, G.; Paganelli, S.; Botteghi, C. *Tetrahedron Lett.* **2000**, *41*, 3717−3720.
(17) Takano, T. *J. Mol. Biol.* **1977**, *110*, 537−568.

10.1021/ic0498539 CCC: $27.50
Published on Web 03/26/2004

Scheme 1. Noncovalent Fixation of Fe^{III}(Schiff-Base) Complexes in the Active Site of Mb

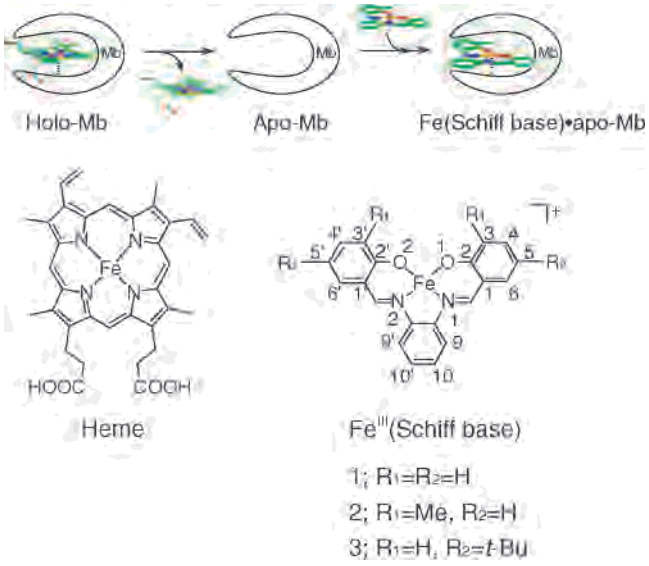

tion of the heme iron to the proximal His93 ligand.[18] On the other hand, we have reported a novel strategy for the construction of artificial metalloproteins by noncovalent insertion of a chromium cofactor into apo-Mb, i.e., the utilization of both proximal histidine (His93) as the axial ligand for the metal complexes and specific interactions between metal ligands and the heme cavity.[19] Furthermore, reactivity and stability of these metalloproteins have been shown to be regulated by changing the protein structure of the metal binding site. The binding affinity of Cr^{III}(Schiff-base) for apo-Mb has increased by the replacement of alanine 71 to glycine. In addition, distal histidine (H64) in Mb was replaced with an aspartic acid for providing a polar substrate binding site in Cr^{III}(Schiff-base)•apo-Mb. The resulting Cr^{III}(5, 5′-*t*-Bu_2-salophen)•apo-H64D/A71GMb was capable of catalyzing asymmetric sulfoxidation of thioanisole.[19] While we have successfully inserted non-heme synthetic metal cofactors, which were designed on the basis of these two factors, into apo-Mb, there is little structural information on their binding structure.[19] In this paper, we describe the design and screening of Schiff-base ligands in order to improve the thermal stability and cyanide binding property of Fe^{III}(Schiff-base)•apo-Mbs (Scheme 1) and the crystal structures of **2·apo-Mb** and **2·apo-A71GMb** to explore basic principles for the noncovalent construction and reactivity of artificial metalloproteins.

Results and Discussion

Preparation of Fe^{III}(Schiff-base)·apo-Mb. Reconstitution of Fe^{III}(Schiff-base)•apo-Mb was carried out according to the reported method with some modifications.[19,20] In order to accelerate the binding of **1** to apo-Mb, the chloride ion of **1·Cl** was removed with $AgBF_4$ in methanol.[21] The resulting methanol solution of **1** was added to a buffer solution of apo-Mb (10 mM Tris/HCl, pH 7.0), and then, the mixture was stirred for 10 min at 4 °C. After dialysis against the same buffer solution, **1·apo-Mb** was purified by G-25 and CM52 columns. The 1:1 composites of apo-Mb and apo-A71GMb with the other iron complexes, **2** and **3**, were also synthesized by the same manner and characterized by several spectroscopies described below. Purified **1·apo-Mb** was stable under aerobic conditions for several weeks, and no conversion of the Fe(III) complexes to μ-oxo dimer was observed although reported Fe(III) Schiff-base complexes in organic solvents are immediately converted to the corresponding dimer under aerobic conditions.[22]

Table 1. Summary of X-ray Data and Refinement Statistics for **2·Apo-Mb** and **2·Apo-A71GMb**

	2·apo-Mb	**2·apo-A71GMb**
Crystallographic Statistics		
space group	$P2_12_12_1$	$P2_12_12_1$
unit cell (Å)		
a, *b*, *c*	33.05, 58.82, 75.62	33.27, 57.60, 75.30
resolution (Å)[a]	40.0−2.1 (2.18−2.10)	40.0−1.60 (1.66−1.60)
total observations	73324	323196
unique reflns	8790	19013
completeness (%)[a]	96.1 (94.0)	95.7 (87.3)
R_{merge} (%)[a,b]	7.4 (23.2)	9.7 (29.3)
$I/\sigma(I)$[a]	19.6 (4.4)	41.7 (6.8)
molecules per asymmetric unit	1	1
Refinement Statistics		
resolution (Å)	30.3−2.1	24.93−1.60
no. reflns		
working set/test set	7385/439	17790/917
R-factor (%)[c]	20.7	19.8
R_{free} (%)[d]	24.8	21.2
rms deviation		
bonds (Å)	0.006	0.005
angles (deg)	1.8	1.8
dihedrals (deg)	18.1	17.6
improper (deg)	0.75	0.67
Ramachandran plot (%)[e]		
most favored	86.2	90.5
allowed	13.8	9.5
final model		
no. residues	154	154
no. Fe^{III}(3,3′-Me_2-saplohen)	0	1
no. water molecules	156	201
no. phosphate ions	6	6

[a] Values in parentheses are for the highest resolution shell. [b] $R_{merge} = \sum|I - \langle I\rangle|/\sum I$, where I is the integrated intensity of a given reflection. [c] *R*-factor $= \sum||F_o| - |F_c||/\sum|F_o|$, where F_o and F_c are the observed and calculated structure factor amplitudes, respectively. [d] R_{free}: an *R* factor calculated on a partial set that is not used in the refinment of the structure. [e] Ramachandran plot parameters were calculated using *PROCHECK*.[25]

Crystal Structures of 2·Apo-Mb and 2·Apo-A71GMb. Crystal structures of **2·apo-Mb** and **2·apo-A71GMb** were refined with the diffraction data of 2.1 and 1.6 Å resolution, respectively. The X-ray data and refinement statistics for the structures are listed in Table 1. As shown in Figure 1a, the iron complex **2** is fixed in the heme cavity of apo-A71G Mb. The Nϵ atom of proximal His93 ligates to the iron with an Fe−N distance of 2.30 Å which is slightly longer than

(18) Hunter, C. L.; Lloyd, E.; Eltis, L. D.; Rafferty, S. P.; Lee, H.; Smith, M.; Mauk, A. G. *Biochemistry* **1997**, *36*, 1010−1017.
(19) Ohashi, M.; Koshiyama, T.; Ueno, T.; Yanase, M.; Fujii, H.; Watanabe, Y. *Angew. Chem., Int. Ed.* **2003**, *42*, 1005−1008.
(20) Wagner, U. G.; Muller, N.; Schmitzberger, W.; Falk, H.; Kratky, C. *J. Mol. Biol.* **1995**, *247*, 326−337.
(21) Gullotti, M.; Casella, L.; Pasini, A.; Ugo, R. *J. Chem. Soc., Dalton Trans.* **1977**, 339−345.
(22) Kennedy, B. J.; Brain, G.; Horn, E.; Murray, K. S.; Snow, M. R. *Inorg. Chem.* **1985**, *24*, 1647−1653.

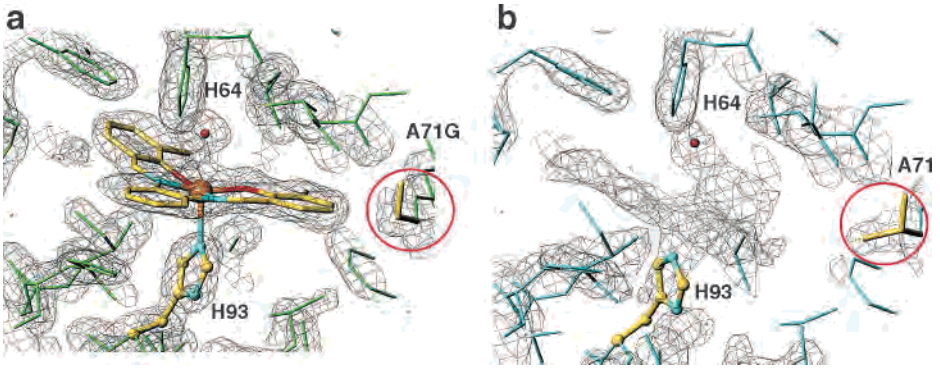

Figure 1. The electron-density maps of **2·apo-A71GMb** (a) and **2·apo-Mb** (b). The final models are superimposed on the maps.

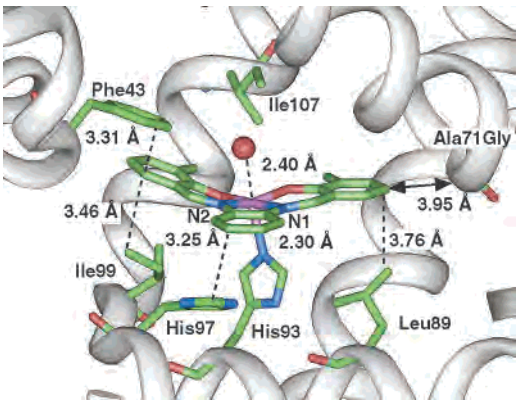

Figure 2. The active site structure of **2·apo-A71GMb**.

Fe−N distances in $[Fe^{III}(3,3'\text{-}EtO_2\text{-salen})(5\text{-Ph-Im})(H_2O)]^+$ (2.13 Å) and met-Mb (2.17 Å).[17,22] The distance between the iron atom and the oxygen atom of coordinated water (2.40 Å) is also longer than Fe−O(H_2O) in $[Fe^{III}(3,3'\text{-}EtO_2\text{-salen})\text{-}(5\text{-Ph-Im})(H_2O)]^+$ (2.21 Å) and met-Mb (2.10 Å).[17,22] The distances of the iron atom to the imine nitrogen atoms in Fe(III) Schiff-base complexes are sensitive to its spin-state.[22] The iron−nitrogen bonds in **2·apo-A71GMb**, Fe−N1 (1.99 Å) and Fe−N2 (2.15 Å) (Figure 2), suggest the metal ion to be in the high-spin state, and it is consistent with the ESR results described below. On the other hand, a remarkable difference is observed for the electron density of **2** in the active site of **2·apo-Mb** (Figure 1b); i.e., we are not able to determine the unique location of the metal complex even though other spectroscopic data of **2·apo-Mb** support the incorporation of **2** in apo-Mb.

The orientation of **2** in the cavity of apo-A71GMb is constrained by several specific interactions as shown in Figure 2. Phe43, Leu89, His97, and Ile99 are close to **2** within the distances of $\pi-\pi$ and CH$-\pi$ interactions.[23] The 3- and 3′-methyl groups in the ligand, which are close to Ile107, allowed the iron atom, and Nϵ atoms of His64 and His93, to be captured deeper in the heme pocket (1.36, 1.14, and 1.14 Å, respectively) than those of native met-Mb (Figure 3).[17] At the same time, the C5 atom is close to the Cα atom of Ala71Gly with a distance of 3.95 Å as shown in Figure 2. The close location of the C5 atom to Ala71 was predicted in our molecular modeling study, and this is the reason we have prepared the Ala71Gly mutant. These interactions cooperatively make **2** rigidly bound in the active site.

The root-mean-square deviation (RMSD) of backbone atoms of **2·apo-A71GMb** from native met-Mb is only 0.62 Å. The value is similar to those of Fe(III)porphin·apo-Mb (0.77 Å) and biliverdin·apo-Mb (0.60 Å).[20,24] Although large *B*-factor values are shown in the region of residues 40−60 and 80−100, which constitute the heme cavity (Figure 4), small tertiary structural deviation from native Mb suggests that apo-A71GMb is capable of holding non-native prosthetic groups in the heme cavity without serious structural perturbation. On the other hand, the **2·apo-Mb** structure is problematic, while it provides useful insights into the nature of the binding of **2**. The protein portion in the crystal structure of **2·apo-Mb** is well-defined, and it is similar to that of native met-Mb (RMSD = 0.68 Å). In particular, although His64 and Ala71, which are close to **2**, are clearly defined, the electron densities of the 3,3′-Me_2-salophen ligand and the iron atom appear to be distributed in the cavity (Figure 1b). In addition, the *B*-factor values at the positions 80−100 are much larger than those of **2·apo-A71GMb** (Figure 4). The results suggest that **2** and the ligated imidazole of His93 are moving around in apo-Mb or take several conformations.

Relative Binding Affinity of Fe(III) Schiff-Base Complexes with Apo-Mb. Electrospray ionization time-of-flight mass spectrometry (ESI-TOF MS) has been used to determine relative binding affinity between biomolecules and metal complexes.[26] In order to compare the affinity of Fe^{III}-(Schiff-base) with apo-Mb, competitive reconstitution was studied by ESI-TOF MS. The mass spectrum of the mixture of **1**, **2**, **3**, and apo-Mb in 5 mM ammonium acetate buffer (pH 6.4) gave three peaks corresponding to **1·apo-Mb**, **2·apo-Mb**, and **3·apo-Mb**, and the peak intensities are in the order of **2** > **1** > **3** as shown in Figure 5. On the basis of relative peak intensity of the noncovalent composites, we have concluded the order of binding preference to be **2** > **1** > **3**. On the other hand, the competition study for apo-Mb and apo-A71GMb with **1** showed that the peak intensity of **1·apo-Mb** was almost same as that of **1·apo-A71GMb** (data not shown). The results suggest that the substituents on

(23) Nishio, M.; Hirota, M.; Umezawa, Y. *THE CH/π INTERACTION Evidence, Nature, and Consequences*; Wiley-VCH: New York, 1998.
(24) Neya, S.; Funasaki, N.; Sato, T.; Igarashi, N.; Tanaka, N. *J. Biol. Chem.* **1993**, *268*, 8935−8942.
(25) Laskowski, R. A.; MacArthur, M. W.; Moss, D. S.; Thornton, J. M. *J. Appl. Crystallogr.* **1993**, *26*, 283−291.
(26) Kapur, A.; Beck, J. L.; Brown, S. E.; Dixon, N. E.; Sheil, M. M. *Protein Sci.* **2002**, *11*, 147−157.

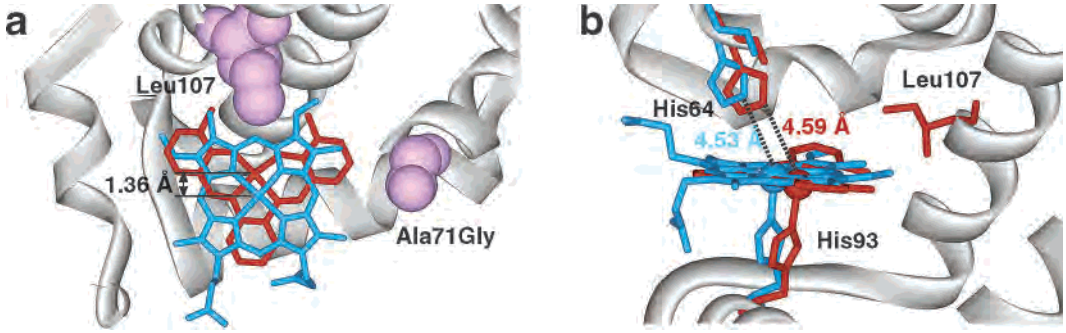

Figure 3. The superimposed structures of **2·apo-A71GMb** (red) and met-Mb (blue) (a; top view, and b; side view). The crystal structure of met-Mb is taken from PDB 4MBN.

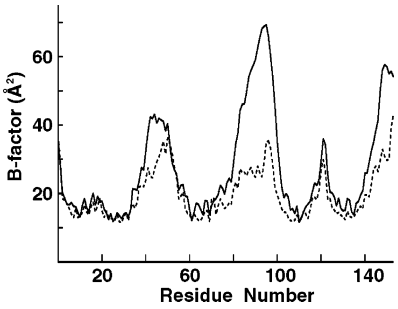

Figure 4. *B*-factor values of Cα atoms for **2·apo-Mb** (—) and **2·apo-A71GMb** (- - -).

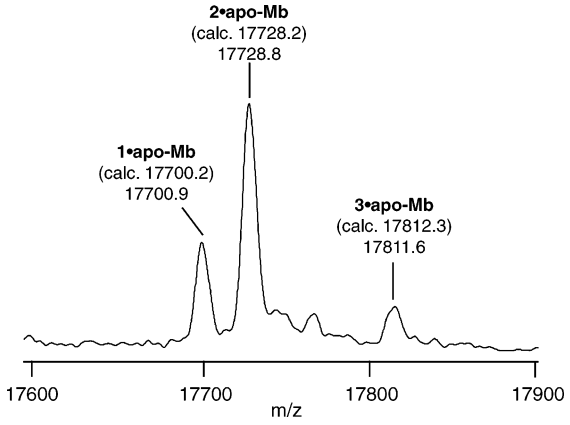

Figure 5. The ESI-TOF mass spectrum of apo-Mb reconstituted by a mixture of **1**, **2**, and **3**. Concentrations of **1**, **2**, **3**, and apo-Mb were 10, 10, 10, and 30 μM, respectively (5 mM ammonium acetate buffer, pH 6.4).

Schiff-base ligands are effective for the complexation with apo-Mb.

Thermal Stability. In order to investigate the effect of Schiff-base ligand structure on the thermal stability, melting temperatures (T_m) of purified Fe^{III}(Schiff-base)·apo-Mbs were determined by circular dichroism (CD) spectral measurements at various temperatures (Table 2). Melting temperatures of reconstituted apo-Mbs with **1** (68.1 °C) and **2** (69.7 °C) are higher than that of apo-Mb (67.2 °C). In contrast, the thermal stability of **3·apo-Mb** (67.0 °C) is almost identical to that of apo-Mb. The order of the thermal stability of Fe^{III}(Schiff-base)·apo-Mbs is, therefore, **2** > **1** > **3**. The results are in good agreement with the relative peak intensity in the ESI-TOF mass spectrum of apo-Mb reconstituted with a mixture of **1**, **2**, and **3** (Figure 5). Although T_m of **2·apo-Mb** is higher than that of **2·apo-A71GMb**, the gain of T_m for **2·apo-A71GMb** from apo-A71GMb (2.7 °C) is almost comparable to that of **2·apo-Mb** from apo-Mb (2.5 °C).

Table 2. T_m of Fe^{III}(Schiff-base)·apo-Mbs[a]

	T_m, °C
1·apo-Mb	68.1
2·apo-Mb	69.7
3·apo-Mb	67.0
Apo-Mb	67.2
2·apo-A71GMb	64.2
Apo-A71GMb	61.5

[a] Concentration of protein samples was 2.5 μM in 1 mM Tris/HCl buffer (pH 7.0) placed into a quartz cell (1 cm path length), and ellipticity was recorded at 222 nm from 25 to 95 °C with a heating rate of 50 °C/h.

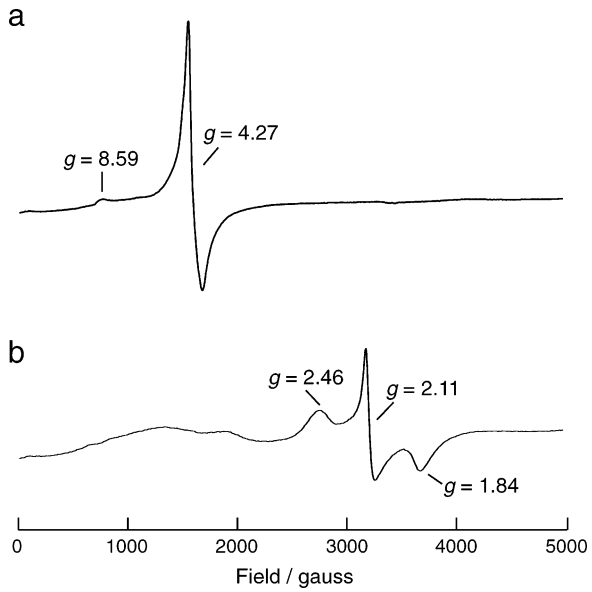

Figure 6. The EPR spectra of **2·apo-A71GMb** (0.6 mM) before (a) and after (b) addition of 100 equiv of KCN at 5 K in 10 mM Tris/HCl (pH 7.0).

EPR Spectra. EPR spectra of Fe^{III}(Schiff-base)·apo-Mbs were measured at 5 K in 10 mM Tris/HCl buffer (pH 7.0) (Figure 6 and Table 3). The EPR spectrum of **2·apo-A71GMb** shows typical high-spin iron(III) signals at g = 4.27 and 8.59 (Figure 6a). **1·apo-Mb**, **2·apo-Mb**, and **3·apo-Mb** also show almost identical spectra (Table 3). These spectra are very similar to that of [Fe^{III}(3,3′-EtO_2-salen)(5-Ph-imd)(H_2O)]BPh_4·0.5H_2O in CH_2Cl_2.[22] On the other hand, complex **1** without apo-Mb is EPR silent in the

Table 3. EPR g Values of Fe^{III}(Schiff-base)·apo-Mbs[a] and Their Complexes with CN^-

	Fe^{III}(Schiff-base)·apo-Mb		cyanide complex[b]		
1·apo-Mb	8.48	4.23	2.48	2.13	1.86
2·apo-Mb	8.38	4.25	2.48	2.12	1.89
3·apo-Mb	8.13	4.24	2.44	2.14	1.90
2·apo-A71GMb	8.59	4.27	2.46	2.11	1.84

[a] Conditions: [Fe] = 0.6 mM in 10 mM Tris/HCl (pH 7.0) at 5 K. [b] 100 equiv KCN was added to Fe^{III}(Schiff-base)·apo-Mb.

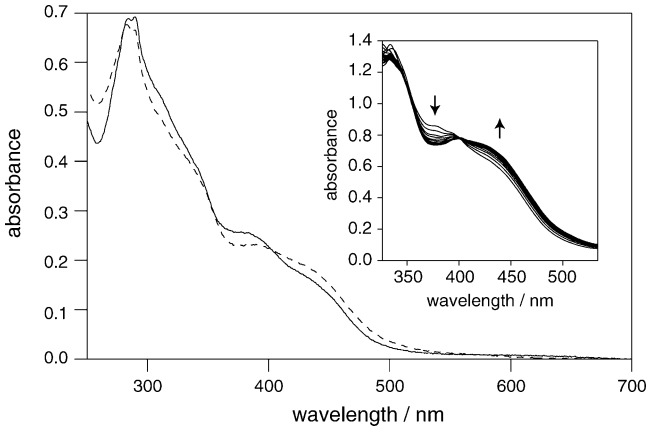

Figure 7. UV−vis spectral changes of **2·apo-A71GMb** (—) upon the addition of 100 equiv. KCN in 10 mM Tris/HCl buffer at pH 7.0 (- - -). Time dependent spectral changes of the same reaction are shown in inset (every 130 ms).

same buffer solution under aerobic conditions because of the dimer formation. Furthermore, these high-spin signals disappeared when 100 equiv of KCN was added with concomitant appearance of three new signals with g values in the range 1.8−2.5 assigned to low-spin species (Figure 6b and Table 3). A similar spectral change from high-spin to low-spin by the addition of KCN was reported for holo-Mb.[27] These results suggest that the high-spin signals of the Fe^{III}-(Schiff-base) complexes are attributed to the binding of His93 of apo-Mb in the buffer solution.

Kinetics of Cyanide Binding. In order to investigate effects of ligand modification and an amino acid replacement on the reactivity of Fe^{III}(salophen)·apo-Mbs, the rates of cyanide binding to Fe^{III}(salophen)·apo-Mbs were determined by stopped-flow measurements. The absorption spectral changes of **2·apo-A71GMb** upon the addition of KCN are shown in Figure 7. Within 1 min after the mixing, a new peak appeared at 443 nm with an isosbestic point at 403 nm. The absorption spectral change corresponds to the formation of cyanide-bound **2·apo-A71GMb** as characterized by EPR spectroscopy. Interestingly, the cyanide association rate constant of **2·apo-A71GMb** (475 M^{-1} s^{-1}) is 216-fold larger than that of **2·apo-Mb** (2.2 M^{-1} s^{-1}). In the case of holo-Mb, the rate-determining step for the cyanide binding is known to be the deprotonation of HCN by distal histidine, since the major form of cyanide ion is protonated at neutral pH ($pK_a \sim 9$).[28] Thus, the distance of Fe−N^e-(His64) is an important factor for His64 to play as a general base. The crystal structure of **2·apo-A71GMb** shows that the geometry of His64 and the iron atom is almost identical to that of met-Mb (Figure 3b).[17] On the other hand, the metal complex in **2·apo-Mb** appears to be deviated from the ideal geometry because of disorder in the heme pocket while the location of distal histidine (His64) is well resolved in the crystal structure (Figure 1b). Thus, His64 in **2·apo-Mb** could be a less effective base to assist the cyanide binding than His64 in **2·apo-A71GMb**. The cyanide binding rate constant of **1·apo-Mb** is 100- and 30-fold larger than those of **2·apo-Mb** and **3·apo-Mb**, respectively (Table 4). We need further investigation, including X-ray crystallography, to understand the interactions of the metal complexes with apo-Mb and the cyanide binding.

Table 4. Cyanide Binding Rate Constants to Fe^{III}(Schiff-base)·apo-Mbs[a]

	$k_{on}/M^{-1}\cdot s^{-1}$
2·apo-A71GMb	475
1·apo-Mb	202
2·apo-Mb	2.2
3·apo-Mb	7.3

[a] Concentration of protein samples was 2.5 μM in 10 mM Tris/HCl buffer (pH 7.0) at 25 °C.

Conclusions

Apo-Mb has been rationally designed to improve cyanide binding to the Fe^{III}(Schiff-base) complexes fixed in the active site. The crystal structures of **2·apo-A71GMb** and **2·apo-Mb** provided new insight into the cyanide binding and the interactions of the Fe(III) complex with apo-Mb. The minimization of steric hindrance as well as the maximization of hydrophobic interactions regulates the binding and the location of the metal complex in the protein matrix. The tight binding of the complexes in protein matrixes affects the reactivities, such as cyanide binding, of the metal complexes.

Experimental Section

Materials. Reagents were purchased from Wako, Nakarai Tesque, and Aldrich and used without further purification. The expression vector for wild type of sperm whale Mb is a gift from Prof. John Olson (Rice University). The expression and purification of Mb were performed according to a method described by Springer et al. with some modification.[29] Apo-Mb was prepared using an acid-butanone method.[30]

Preparation of Iron(III) Schiff-Base Complexes. Schiff-base ligands and their iron(III) complexes were prepared by literature methods.[31−34] The yield, mass data, and ^{1}H NMR of each Schiff-base ligand and the corresponding iron(III) complexes are as

(27) Paul, M. A. G.; Andrew, J. T. *J. Am. Chem. Soc.* **1990**, *112*, 5003−5011.
(28) Brancaccio, A.; Cutruzzola, F.; Allocatelli, C. T.; Brunori, M.; Smerdon, S. J.; Wilkinson, A. J.; Dou, Y.; Keenan, D.; Ikeda-Saito, M.; Brantley, R. E. J.; Olson, J. S. *J. Biol. Chem.* **1994**, *269*, 13843−13853.
(29) Springer, B. A.; Sligar, S. G. *Proc. Natl. Acad. Soc.* **1987**, *84*, 8961−8965.
(30) Ascoli, F.; Fanelli, M.; Antonini, E. *Methods Enzymol.* **1981**, *76*, 72−87.
(31) Chen, H.; Cronin, J. A.; Archer, R. D. *Macromolecules* **1994**, *27*, 2174−2180.
(32) Ciringh, Y.; Gordon-Wylie, S. W.; Norman, R. E.; Clark, G. R.; Weintraub, S. T.; Horwitz, C. P. *Inorg. Chem.* **1997**, *36*, 4968−4982.
(33) Fitzsimmons, B. W.; Smith, A. W.; Larkworthy, L. F.; Rogers, K. A. *J. Chem. Soc., Dalton Trans.* **1973**, 676−680.

follows. **Salophen-H_2**: yield 87%. *m*/*z* (ESI-TOF): 317.1 (calcd 316.1),. ^{1}H NMR δ 13.02 (s, 2H), 8.64 (s, 2H), 7.40−7.33 (m, 6H), 7.26−7.23 (m, 2H), 7.04 (d, J = 8.1 Hz, 2H), 6.92 (t, J = 7.5 Hz, 2H). **3,3′-Me_2-salophen-H_2**: yield 80%. *m*/*z* (ESI-TOF): 345.1 (calcd 344.1). ^{1}H NMR δ 13.20 (s, 2H), 8.62 (s, 2H), 7.36−7.30 (m, 2H), 7.26−7.17 (m, 6H), 6.83 (t, J = 7.5 Hz, 2H), 2.29 (s, 6H). **5,5′-*t*-Bu_2-salophen-H_2**: yield 82%. *m*/*z* (ESI-TOF): 429.2 (calcd 428.2), ^{1}H NMR δ 12.85 (s, 2H), 8.64 (s, 2H), 7.41 (dd, J = 8.7, 2.7 Hz, 2H), 7.35 (s, 2H), 7.34−7.30 (m, 2H), 7.25−7.19 (m, 2H), 6.99 (d, J = 8.6 Hz, 2H), 1.29 (s, 18H). **1·Cl**: yield 30%. *m*/*z* (ESI-TOF): 370.02 (calcd 370.04). **2·Cl**: yield 58%. *m*/*z* (ESI-TOF): 398.01 (calcd 398.07). **3·Cl**: yield 59%. *m*/*z* (ESI-TOF): 482.09 (calcd 489.17).

Preparation of Iron(III) Schiff-Base Complex·apo-Mb. To **1·Cl** (12 mL, 25 mM) in methanol was added a methanol solution of $AgBF_4$ (1.2 mL, 367 mM). The mixture was stirred at 50 °C for 3 h, and then, precipitated AgCl and Ag^+ ion were removed by Celite filtration. The eluent containing **1·BF_4** was diluted with methanol to 10 mM. The methanol solution of **1·BF_4** (1 mL, 10 mM) was slowly added to an apo-Mb solution (14 mL, 0.3 mM in 10 mM Tris/HCl buffer, pH 7.0) and gently stirred at 4 °C for 10 min. The mixture was dialyzed against 10 mM Bis-tris buffer (pH 6.0) at 4 °C for 6 h. After the dialysis, the mixture was passed through Sephadex G-25 equilibrated with 10 mM Tris/HCl buffer (pH 7.0), and then purified with HiTrap CM FF on an ÄKTA explorer 100 FPLC system (Amersham Biosciences) with linear gradient (10−500 mM Tris/HCl buffer, pH7.0). **1·apo-Mb**: yield 28%. ESI-TOF MS: 17700.9 (calcd 17700.2). UV−vis (10 mM Tris/HCl buffer, pH 7.0) λ/nm (ϵ/M^{-1} cm^{-1}): 282 (51000), 289.5 (47200), 326.5 (23100), 376 (15400). **2·apo-Mb** and **3·apo-Mb** were also prepared by the same method. **2·apo-Mb**: yield 20%. ESI-TOF MS: 17728.8 (calcd 17728.2). UV−vis (10 mM Tris/HCl buffer, pH 7.0) λ/nm (ϵ/M^{-1} cm^{-1}): 283.5 (65900), 289 (65200), 324.5 (41800), 380.5 (22100). **3·apo-Mb**: yield 11%. ESI-TOF MS: 17811.6 (calcd 17812.3). UV−vis (10 mM Tris/HCl buffer, pH 7.0) λ/nm (ϵ/M^{-1} cm^{-1}): 282.5 (154600), 291 (130300), 341.5 (38700), 410 (24700). **2·apo-A71GMb**: yield 3%. ESI-TOF MS: 17715.7 (calcd 17715.2). UV−vis (10 mM Tris/HCl buffer, pH 7.0) λ/nm (ϵ/M^{-1} cm^{-1}): 289.5 (78500), 384.5 (29800).

Physical measurements. UV−vis spectra were recorded on a SHIMADZU UV-2400PC UV−vis spectrophotometer. ^{1}H NMR spectra were recorded on a JEOL JNM-EX 270 spectrometer.

Atomic Absorption Spectrometry. Iron concentration in Fe^{III}-(Schiff-base)·apo-Mb was determined by a polarizing Zeeman-effect atomic absorption spectrophotometer Z-5710 (HITACHI) operating in graphite furnace mode using an Fe hollow cathode lamp. Iron ion was detected at 248.3 nm with a slit width of 0.2 nm. $Fe^{III}(NO_3)_3$ in 0.1 M HNO_3 (99.8 mg/l, Wako) was used as a calibration standard.

EPR Measurements. EPR spectra were recorded on an E500 X-band CW-EPR (Bruker). A cryostat (ITC503, Oxford) was used for the observation at 5 K. EPR absorption spectra of iron(III) Schiff-base complex·apo-Mb (0.6 mM, 10 mM Tris/HCl buffer, pH7.0) and their cyanide bound derivatives were measured at 5 K. The cyanide bound samples were prepared by addition of 100 equiv of KCN (0.1 M, 10 mM Tris/HCl buffer, pH 7.0) to a solution of iron(III) Schiff-base complex·apo-Mb (0.6 mM, 10 mM Tris/HCl buffer, pH 7.0). The reaction mixture was then frozen by liquid nitrogen.

Mass Spectrometry. ESI-TOF mass analyses were performed on a Micromass LCT instrument. Typical parameters are as follows: capillary voltage, 3 kV; cone voltage, 60 V; source temperature, 60 °C; flow-rate, 5 μL min^{-1}. CsI (1 mg/mL) in 50% H_2O/CH_3CN was used for mass scale calibration. All samples were dialyzed against 5 mM ammonium acetate buffer (pH 6.7) at 4 °C for 6 h and diluted to 10 μM by the same buffer solution.

Kinetic Measurements for the Association of Cyanide. Reactions of reconstituted Mbs with cyanide were measured at 395−408 nm on a UNISOK stopped-flow apparatus in 10 mM Tris/HCl buffer (pH 7.0). The association rate constants were given by the slope of a plot of the observed rates versus cyanide concentration.

Analysis of Thermal Stability. Circular dichroism spectra were recorded on a JASCO model J-720 spectropolarimeter that was equipped with a JASCO model PTC-348WI Peltiert cooling temperature controller. Spectropolarimeter and water bath were operated under computer control. Protein samples (2.5 μM in 1 mM Tris/HCl buffer, pH 7.0) were placed into a quartz cell (1 cm path length), and ellipticity was recorded at 222 nm from 25 to 95 °C with a heating rate of 50 °C/h. The midpoint melting temperature (T_m) was determined from the first derivative of the resulting ellipticity versus temperature plot.

MD Calculations. The X-ray structure of sperm whale myoglobin was obtained from the Brookhaven Protein Data Bank (1DUK). All calculations were carried out by using InsightII/Discover program with an ESFF force field.

X-ray Data Collection and Crystallographic Refinement. X-ray data of **2·apo-A71GMb** were collected at 100 K using a Rigaku R-AXIS VII detector system and Rigaku FR-E. X-ray data of **2·apo-Mb** were collected from the crystals at 100 K using a Rigaku R-AXIS IV detector system and Rigaku RU-300 rotating-anode generator with double focusing-mirror monochromated Cu Kα radiation. Both of the collected data sets were processed with *DENZO* and *SCALEPACK*.[35] The crystal parameters and data-collection statistics are given in Table 1.

The Cr^{III}(3,3′-Me_2-salophen)·apo-A71GMb structure (PDB code: 1J3F) with deletion of the Cr^{III}(3,3′-Me_2-salophen) moiety was used as an initial model for the refinement of **2·apo-A71GMb.** The refinement was carried out with a program *CNS*[36] and manual model building with a program TURBO_FRODO. A statistically random selection of about 5% of the total reflection data was excluded from the refinement and used to calculate the free R (R_{free}) as a monitor of model bias.[37] After rigid-body refinement, positional refinement, and B-factor refinement, **2** was positioned manually on omit $|F_o| - |F_c|$ map in the heme cavity. Several subsequent cycles of refinement brought the final R-factor and the R_{free} to 19.8% and 21.2%, respectively. The model was subjected to quality analysis during the various refinement stages with omit maps and *PROCHECK*.[25] The refinement statistics are summarized in Table 1.

An initial model for **2·apo-Mb** was constructed by deleting **2** from **2·apo-A71GMb**. The refinement was also performed with a program *CNS*. Even after several cycles of refinement (R-factor 20.7% and R_{free} 24.8%), the electron density corresponding to **2** was not clear. The refinement statistics are summarized in Table 1. Coordinates have been deposited in the Protein Data Bank under accession codes of 1UFP and 1UFJ for **2·apo-Mb** and **2·apo-A71GMb**, respectively.

(34) Gerloch, M.; Lewis, J.; Mabbs, F. E.; Richards *J. Chem. Soc.* **1968**, 112−116.
(35) Otwinowski, Z.; Minor, W. *Methods Enzymol.* **1997**, *276*, 307−326.
(36) Brünger, A. T.; Adams, P. D.; Clore, G. M.; DeLano, W. L.; Gros, P.; Grosse-Kunstleve, R. W.; Jiang, J. S.; Kuszewski, J.; Nilges, M.; Pannu, N. S.; Read, R. J.; Rice, L. M.; Simonson, T.; Warren, G. L. *Acta Crystallogr., Sect. D* **1998**, *54*, 905−921.
(37) Brünger, A. T. *Acta Crystallogr., Sect. D* **1993**, *49*, 24−36.

Acknowledgment. We thank T. Hikage (High Intensity X-Ray Laboratory, Nagoya University) for help in the X-ray crystal analysis. We also thank Prof. S. Neya for valuable discussions. This work was supported by Grant-in-Aid for Scientific Research (Grant No. 14209019 to Y.W. and 13740384 to T.U.).

IC0498539